LVRT Induced Frequency Stability in Offshore Wind Power System

M. M. Kabsha, *Student Member, IEEE*, and Zakir H. Rather, *Member, IEEE*,
Department of Energy Science& Engineering
Indian Institute of Technology Bombay
Mumbai, India

***Abstract*—Due to high wind speed and high plant load factor in deep oceans, coupled with a saturation of onshore space, offshore wind farms (OWF) are being rapidly integrated into power systems. Several countries are investing more in OWF sector with consistent increase in penetration of voltage source converter-based high voltage DC connected OWF in these countries. Due to significant penetration of OWFs, such countries have developed separate grid code regulations, including low voltage ride-through (LVRT) capability for OWF connection. The OWF, according to LVRT requirement, should stay connected and support the electric grid during LVRT period. One of the critical issues of LVRT capability of HVDC connected OWF is that the OWF cannot inherently detect the faults in the onshore grid, which results in overvoltage in the HVDC link during onshore low voltage faults. Most of the previous LVRT studies on OWF did not consider active power recovery (APR), and none of the reported study has considered voltage dip induced frequency (VDIF) issue. This paper investigates the effect of APR ramp rate on the VDIF response in OWF integrated system. Modified IEEE 39 bus system has been used as a test system and the system performance is evaluated under different case studies, such as, various OWF penetration levels, different fault severity and fault duration.**

Keywords—OWF, VSC-HVDC, Grid code, APR, VDIF

I. INTRODUCTION

High penetration of renewable energy sources in the electric power system makes it more prone to voltage and frequency instability. This requires significant developments of the control systems of these sources to satisfy the grid code regulations (GCR) imposed by system regulators. In wind energy sector, offshore wind farms (OWFs) is one of the promising medium to tap wind energy owing to high wind speeds and high plant load factor in deep oceans [1], with total annual worldwide installed capacity of OWF rapidly increasing year by year [2],[3]. In this paper, voltage source converter-based high voltage direct current (VSC-HVDC) connected OWF is considered, as VSC-HVDC based topology is prevalent in OWF due to its flexibility in decoupled control of active and reactive power control [4]. The OWF according to GCR are required to stay connected and support the onshore grid in case of voltage dip at the point of common coupling (PCC) [5]–[8]. The main issue is that the OWF and the onshore grid are decoupled through the HVDC connection and the OWF cannot inherently detect the onshore grid disturbance. This limitation results in high voltage in the HVDC link due to power imbalance between power transferred to the main grid and the power received from the offshore WTGs during a voltage dip in the main grid. Therefore, to achieve successful LVRT, a signal must be sent to each WTG either by using communication or communication-less strategies to reduce the active power injected to the sending end converter (SEC) through the HVDC link. Several control strategies have been proposed in the literature to enable the OWF maintain power balance during grid faults. The authors in [9] proposed two control strategies in order to mitigate the DC overvoltage during grid faults, the first control strategy is to reduce the WTs generated active power by varying the reference active power set-point by using fast communication system. However, the time delay of communication system may lead to overvoltage at the HVDC link, besides reliability issues due to communication failure. The second control strategy reported in [9] is a communication independent strategy, that maps the faults from the onshore grid to the offshore grid by controlling offshore grid AC voltage thus allowing WTGs to reduce their output power during a voltage dip in the main grid. The authors in [10] also proposed two control strategies, the first control strategy being similar to the second strategy reported in [9]. In the second control strategy proposed in[10] , the HVDC link voltage deviation is mapped to frequency deviation in the offshore AC grid by the sending end converter (SEC). According to this method, each WTG should be provided with frequency sensitive complementary control system to provide fast active power reduction proportional to the offshore frequency deviation. The two control methods in [10] are merged in a single control strategy in [11] by using the AC offshore voltage drop (VD) and frequency regulation (FR) in the same control system. The control system in [11] is a two stage controllers, where the first stage responds to small increase in the HVDC link voltage and adapts FR strategy to decrease WTGs active power output. On the other hand, for a high HVDC link voltage deviation, the second stage is activated which uses VD strategy to decrease the WTGs active power output. The authors in [12] have presented a comparison among different LVRT strategies including DC chopper, VD, FR, and combination of VD and DC chopper strategies. While the main limitation of the offshore FR strategy is its low-speed, DC chopper though has high-speed performance however is of high cost. The VD strategy has high-speed performance but need coordination between control system and undervoltage protection system.

None of these studies considered active power recovery (APR) and voltage dip induced frequency (VDIF) issue

following a fault clearance. The APR ramp rate requirements imposed by system regulators and wind farm operators to decrease the mechanical stresses on the wind turbine mechanical parts, and to ensure voltage stability of the onshore grid after fault clearance. The OWF according to German grid code (Tennet TSO) should restore its active power output to its prefault value with a ramp rate of 0.2 per unit per second, while Great Britain grid code (GB TSO) requires immediate active power restoration with at least 90 % of its prefault value within 0.5 seconds of the restoration of the voltage [6]–[8].

The authors in [13] proposed LVRT strategy based on a combination of braking resistor (DC chopper) and AC offshore voltage reduction, however considering APR ramp rate. It is found that the rate of rise of active power output of receiving end converter (REC) limits applicability of the AC offshore voltage reduction, as with low APR ramp rate, the HVDC link voltage decreases slowly, which affects the offshore grid AC voltage stability. The authors in [13] also considered the onshore grid transient stability under different APR ramp rates. However the main limitations of this study is that it depends on offshore AC voltage dip strategy, which stresses the offshore grid and needs adequate coordination between control system of different components of HVDC connected OWF, and under voltage protection system.

The authors in [14] have considered the APR ramp rate for OWF connected to the grid through point to point VSC-HVDC link, and the authors proposed three LVRT strategies that depend on offshore AC voltage regulation (VR) and FR strategies. The first strategy uses only FR strategy, however, this approach can potentially result in rapid change of the offshore frequency that may results in tripping of frequency sensitive infrastructure connected to the offshore grid. The second strategy combines both VR and FR strategies, where the FR strategy is used for onshore frequency support from the OWF, while the VR strategy is used to achieve LVRT. The third strategy uses only VR strategy to achieve both the frequency response and LVRT by appropriate selection of the HVDC converter control parameters, besides WTG control system being modified to make it more sensitive to small offshore AC voltage deviations for realising fast active power reduction during severe voltage dips at the onshore PCC. The limitations of the study in [14] is that the control strategy has not considered the VDIF response, because the grid model is simplified as a fixed frequency voltage source which cannot capture dynamics of a realistic grid. The APR ramp rate imposed by GCR on the WTGs results in temporary shortfall of generation, which in turn lead to frequency stability issue in the main grid. Hence, it is important to consider fault induced voltage dip followed by frequency excursion while proposing and testing a control strategy for realistic compliance of LVRT.

In this paper, a modified VR LVRT strategy is introduced, and then the impact of the APR ramp rates and wind generation penetration levels on the onshore frequency stability was evaluated. Moreover, the WTG mechanical stress is considered under different test cases with IEEE 39 bus test system.

The rest of the paper is organized as follows: In section II, grid code regulation for LVRT requirements of OWF is briefly outlined. In section III, HVDC connected OWF modeling is discussed, while in section IV, modified LVRT strategy is introduced. In section V, performance of system is evaluated under different case studies.

II. LVRT REGULATION FOR OWF

The literature review suggest that only Germany (Tennet TSO) has separate GCR for OWF connections while Great Britain has requirements for offshore power park modules, (wind, solar, wave) connected to the offshore transmission system [5]–[8]. The LVRT requirement in German grid code as shown in Fig. 1 is intended to ensure that the OWF will remain connected during faults that are outside the protection zone of the OWF (with the voltage–time profile falls within area 1 and 2) [8].

In addition, during voltage dip, OWF should support the onshore grid voltage by injecting reactive current with at least 2 % of the rated current for each percent of the voltage dip [7]. The corresponding voltage control characteristics imposed by Tennet TSO are summarized in Fig. 2.

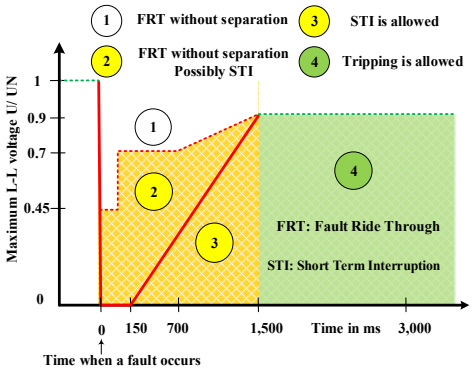

Fig. 1. Fault Ride Through requirements [8]

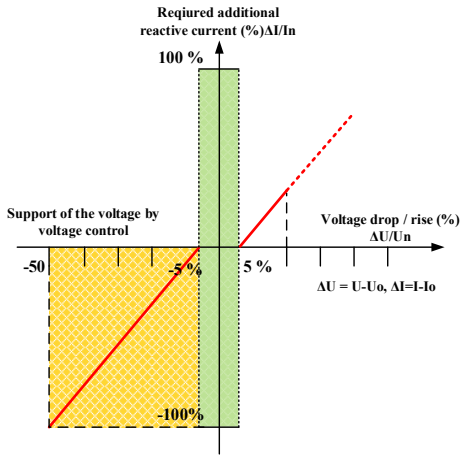

Fig. 2. Characteristic of OWF to support the grid voltage [7]

III. MODELING OF OFFSHORE WIND POWER SYSTEM

The OWFs have been modeled as aggregate model using type- 4 based wind turbine generators of different capacities, and connected to the main grid through HVDC link. Modeling and control systems of the different components of the OWF is demonstrated in the following subsections.

A. *Full Converter WTG*

The overall system of the full converter WTG connected to permanent magnet synchronous generator is shown in Fig. 3. The grid side converter (GSC) control system is employed to regulate the generator speed to extract the maximum possible power from the wind, while the machine side converter (MSC) control the DC-link voltage. The WTG model used in this paper is the GE 1.5 MW full converter wind turbine [15]. Each OWF used in this study is an aggregated model, which is based on the aggregation methodology described in [16], except the generator model.

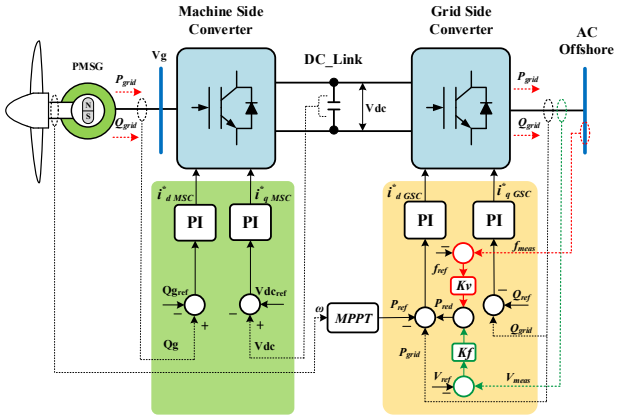

Fig. 3. PMSG WTG Control system

B. *HVDC Converters Control*

The schematic diagram of the HVDC control system is shown in Fig. 4. The SEC maintains the offshore grid voltage and frequency at fixed values to collect the active power from the different WTGs connected to the offshore grid. On the other hand, the REC control system designed to keep the DC voltage of the HVDC constant at the reference value during normal operation. In addition, the REC should satisfy the GCR requirements for onshore grid voltage support during voltage dip faults.

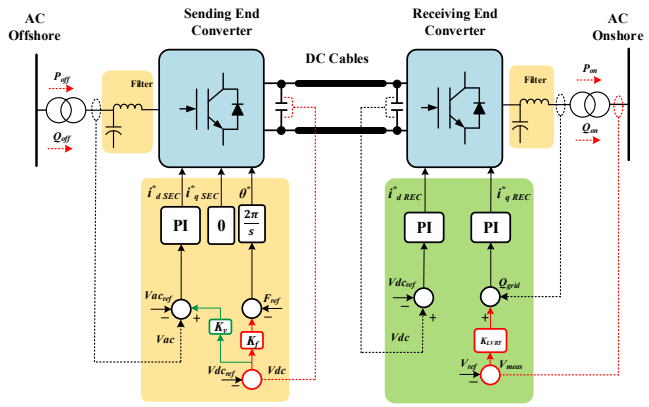

Fig. 4. HVDC Converters Control System

The HVDC link used in this study is the Point-to-Point CIGRE HVDC benchmark system [17]. This system is used as a standard HVDC model for point-to-point and multi terminal studies.

C. *Test System*

The OWF was tested under different onshore grid faults using a modified IEEE 39 bus test system as shown Fig. 5 [18]. The IEEE test system has been modified for 50 Hz system frequency, and the control parameters of each generator in the system were modified to make the test system more suitable for dynamic and transient studies [18]. In the modified IEEE 39 bus system, five OWF of varying capacities are connected at different buses, thus displacing conventional power plants, as detailed in Table I and shown in Fig. 5.

TABLE I. WIND FARMS DETAILS

Wind Farm no	Generator Replaced	No of WTG	Total MW
1	G 4	422	633
2	G10	167	250.5
3	G 7	374	561
4	G 3	434	651
5	G 9	554	831

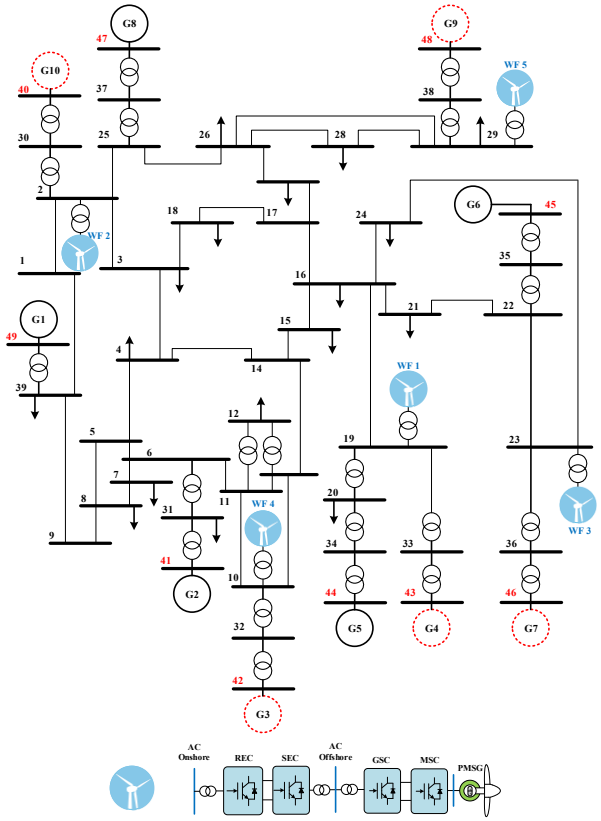

Fig. 5. Modified IEEE 39 Bus Test System [18]

IV. MODIFIED LVRT STRATEGY

The main problem of the OWF during low voltage grid faults is power imbalance at the two sides of the HVDC link, which increases the HVDC-Link voltage to values that can damage the converters, DC cables and capacitor banks. However, with some additional control firmware at the SEC and GSC as shown in Fig. 3 and Fig. 4, the WTG can reduce the generated active power to maintain power balance either by using FR or VR strategies. On the other hand, with the VD strategy, there is no need for supplementary control system at WTG level. REC should also provide voltage support by injecting reactive current according to GCR shown in Fig. 2. The conventional LVRT strategies shown in Fig. 3 and Fig. 4 for the SEC and GSC respectively do not consider active power ramp rate after fault clearance.

The modified FR and VR LVRT strategies with the APR ramp rate control functions are shown in Fig. 6. The REC *d*-axis reference current i_{dref} is modified to achieve the APR ramp rate. The inputs to APR control system are i_{dref} and fault detection signal. The SEC control system provides VR or FR strategies during DC voltage deviations.

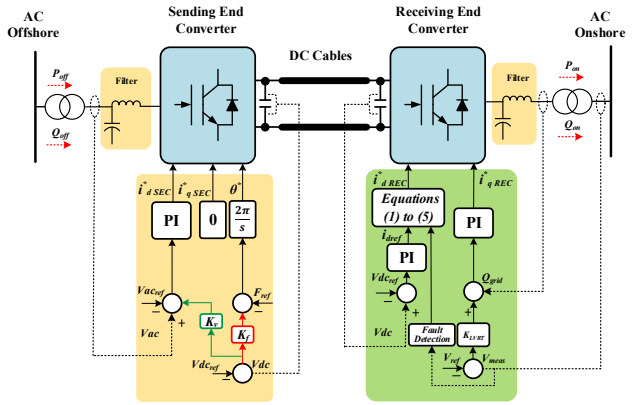

Fig. 6. HVDC Converters Control System with Modified LVRT Strategies

After fault clearance, REC APR ramp rate is activated by the APR ramp activation signal as given in (1).

$$S_{ramp} = \begin{cases} 1 & \left(flt = 0 \ \ and \ \ i^*_{d\ REC} < i_{dref} \ \ and \ \ t_{ramp} < \dfrac{1}{R_{up}} \right) \\ 0 & \left(flt = 1 \ or \ i^*_{d\ REC} = i_{dref} \right) \end{cases} \quad (1)$$

Where *flt* is fault detection signal, $i^*_{d\ REC}$ is the REC *d*-axis current reference value, i_{dref} is the control system *d*-axis current reference value, t_{ramp} is the ramp rate time after fault clearance, and R_{up} is the maximum active power rise rate in p.u/s.

In order to satisfy accurate APR ramp rate, the rate of change of the *d*-axis current reference value i_{dref} is modified to consider the AC voltage variations at the REC PCC, as i_{dref} is kept within the maximum ramp rates in order to comply with GCR as given in (2).

$$\frac{di_d^{ramp}}{dt} = \lim \left(\frac{\left(i_{dref} - i_d^{ramp}\right)}{\Delta t}, \frac{\left(R_{down} - \dfrac{dV_{REC}}{dt} * i_d^{ramp}\right)}{V_{REC}}, \frac{\left(R_{up} - \dfrac{dV_{REC}}{dt} * i_d^{ramp}\right)}{V_{REC}} \right) \quad (2)$$

Where i_d^{ramp} is *d*-axis current as a function of time, Δt is the time step and R_{down} is the maximum active power reduction rate in p.u/s, and V_{REC} is the measured AC voltage at the REC terminal.

Equation (3) gives the *d*-axis current reference value as function of time i_d^{ref} as during ramp time t_{ramp} it follows i_d^{ramp} and returns to steady state value i_{dref} generated by the PI controller after APR.

$$i_d^{ref} = \begin{cases} i_d^{ramp} & S_{ramp} = 1 \\ i_{dref} & S_{ramp} = 0 \end{cases} \quad (3)$$

The maximum *d*-axis current limits i_{dmax} are given in (4), which provides reactive power priority during grid fault to comply with followed GCR.

$$i_{dmax} = \begin{cases} \sqrt{\left(i_{\max}\right)^2 - \left(i^*_{q\ REC}\right)^2} & V_{onshore} < 0.9 \\ i_{max} & V_{onshore} \geq 0.9 \end{cases} \quad (4)$$

Where i_{max} is the REC maximum current value, $i^*_{q\ REC}$ is the REC *q*-axis current reference value, and $V_{onshore}$ is the measured AC voltage at the onshore PCC.

The REC *d*-axis current reference value $i^*_{d\ REC}$ during fault follows the maximum *d*-axis current limits i_{dmax}, and after fault clearance it follows the *d*-axis current reference value i_d^{ref} as demonstrated in (5).

$$i^*_{d\ REC} = \begin{cases} i_{dmax} & flt = 1 \\ i_d^{ref} & flt = 0 \end{cases} \quad (5)$$

The objectives of the REC control during grid faults, is to support the grid voltage by injecting reactive current as required by GCR, as shown in Fig. 2. The German grid code regulation is followed in this paper, which prioritises reactive current injection at PCC during grid fault as given in(6), while the maximum active current from the remaining margin is required to be injected to the grid as calculated from (4).

$$i^*_{q\ REC} = \begin{cases} K_{LVRT}\left(V_{ref} - V_{onshore}\right) & flt = 1 \\ 0 & flt = 0 \end{cases} \quad (6)$$

Where K_{LVRT} is the reactive current droop factor, $V_{onshore}$ is the measured voltage at the onshore PCC, and V_{ref} is the onshore AC voltage reference value.

V. Results and Discussion

The modified IEEE 39 bus system was tested under different scenarios with various OWF penetration levels, different fault severity and fault duration. The VR strategy has been implemented and tested under the mentioned scenarios. The main limitations of FR strategy is that it results in high frequency deviations and higher RoCoF in the offshore grid that can potentially trip frequency sensitive infrastructure in the offshore grid.
The entire system has been developed in DIgSILENT PowerFactory platform.

A. Test Case I

In the first test case, the system is evaluated under a three-phase fault event at bus 16 with 70 % voltage dip for 500 milliseconds, and wind generation penetration level of 33%. The performance of the system under different APR ramp rates is shown in Fig. 7. The total accumulative REC active power injected to the grid with different APR ramp rates is shown in Fig. 7 (b). The REC active power injected to the

grid during the fault depends mainly on the retained voltage at PCC and APR ramp rate used, while after fault clearance, active power injection is limited by APR ramp rate used. The total accumulative SEC active power injected to the HVDC link with different APR ramp rates is shown in Fig. 7 (c).

It can be observed from Fig. 7 (d) that the VDIF response is improved by increasing the APR ramp rate, as the onshore center of inertia frequency 'f_{COI}' nadir with high APR ramp rate is improved compared to that with low APR ramp rate as detailed in Table II. Moreover, corresponding RoCoF decreased by increasing the APR ramp rate. REC satisfy the voltage support requirements during the fault by injecting reactive power according to GCR with the different APR ramp rates. The total accumulative reactive power injected to the onshore grid is shown in Fig. 7 (f).

It can be realized from Fig. 7 (g) that due to sudden power imbalance, the HVDC link voltage increased suddenly at the instant of the onshore grid fault, which decreases to the reference value at different slopes depending on the APR ramp rate used. It is observed from Fig. 7 (h) that the HVDC link voltage deviations is continuously converted to AC voltage deviations at the offshore grid by the SEC to achieve active power reduction during the fault and satisfy APR ramp rate after fault clearance.

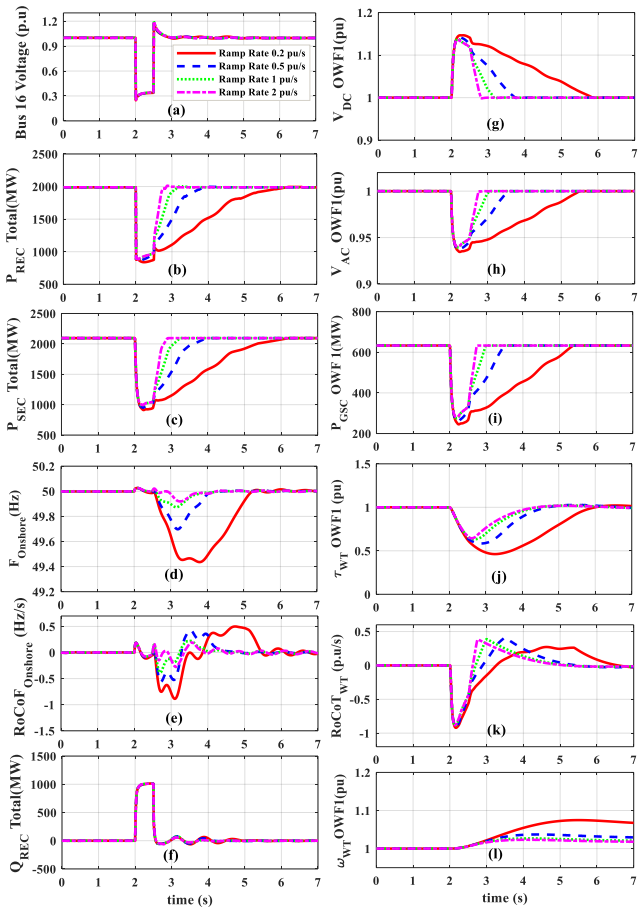

Fig .7 System performance under case study-I. (a) Bus 16 Voltage, (b) REC Active Power, (c) SEC Active Power, (d) Onshore frequency, (e) RoCoF of onshore frequency, (f) REC Reactive Power, (g) Offshore DC Voltage of OWF 1, (h) Offshore AC voltage of OWF 1, (i) WTGs GSC Active Power (j) WTG Mechanical Torque, (k) RoCoT of WTG, (l) WTG rotational speed

On the WTGs side, the performance of WTGs in OWF no 1 is shown in Fig. 7 (i) to (l). Each WTG GSC reduces its active power output depending on the AC voltage measured at the WTG terminal as shown in Fig. 7 (h) to (i). The GSC active power starts recovering after fault clearance at different slopes depending on the APR ramp rate used as shown in Fig. 7 (i). The mechanical torque nadir and the rate of change of torque RoCoT of WTGs with different APR ramp rates are shown in Fig 7 (j), (k). It can be observed from Fig 7 (j), that the mechanical torque nadir of WTG with high APR ramp rate is better (lower) than that with low APR ramp rate as detailed in table II. On the other hand, the RoCoT increased by increasing the APR ramp rate, but it decreases slightly at high APR ramp rate as shown in Fig 7 (k) and detailed in table II. The WTG rotational speed with low APR ramp rate is higher than that with high APR ramp rate as shown in Fig 7 (l), hence, at low ramp rate the RoCoT is maintained at low value, but the wind turbine rotational speed deviations increase.

TABLE II. TEST CASE I DETAILS

Ramp Rate	f Nadir (Hz)	RoCoF (Hz/s)	τ Nadir (p.u)	RoCoT (p.u/s)	$\omega_{turbine}$ (p.u)
0.2 p.u /s	49.43	-0.88	0.46	0.27	1.075
0.5 p.u /s	49.69	-0.55	0.58	0.41	1.0378
1 p.u /s	49.87	-0.38	0.63	0.39	1.0275
2 p.u /s	49.92	-0.27	0.644	0.38	1.0235

B. Test Case II

In this test case, a three-phase fault event at bus 16 with 100 % voltage dip for 150 milliseconds, and at wind power penetration level of 46 % is simulated. It can be observed from Fig. 8 that the performance of the system is similar to its performance in the test case-I, however, the VDIF is significantly affected with severe voltage dip fault events and with high wind penetration levels as detailed in table III and shown in Fig. 8 (d). During LVRT period, priority is given to the reactive current, and the maximum active current is calculated using (4), which depends on the voltage dip at the REC terminals.

TABLE III. TEST CASE II DETAILS

Ramp Rate	f Nadir (Hz)	RoCoF (Hz/s)	τ Nadir (p.u)	RoCoT (p.u/s)	$\omega_{turbine}$ (p.u)
0.2 p.u /s	48.9	-1.85	0.33	0.243	1.1
0.5 p.u /s	49.4	-1.7	0.465	0.49	1.05
1 p.u /s	49.7	-1.48	0.57	0.45	1.03
2 p.u /s	49.9	-1.17	0.67	0.35	1.022

REC active power output during the voltage dip is nearly the same under different APR ramp rates as shown in Fig. 8 (b), however, after fault clearance, the REC active power output is recovered at different slopes depending on APR ramp rate used. Total SEC active power injected to the HVDC link has a similar performance like that in the test case-I as shown in Fig. 8 (c). The VDIF response is highly influenced by the APR ramp rate as shown in Fig. 8 (d), and

detailed in Table III. Moreover, onshore grid RoCoF is effectively improved with high APR ramp rates as shown in Fig. 8 (e) and detailed in Table III. Total reactive power injected by REC to the onshore grid is nearly the same with different APR ramp rates as shown in Fig. 8 (f).

In the test case-II the performance of WTGs in OWF& no 1 is shown in Fig. 8 (g) to (l). It has been observed that the performance of WTGs in test case-II is similar to its performance in test case-I, however, in the test case-II, mechanical torque nadir reaches lower values in comparison with corresponding values in the first test case except only with APR ramp rate of 2 p.u/s. It can be observed from table II and table III that the maximum torque , RoCoT and WTG rotational speed performance is slightly improved at high ramp rate (2 p.u/s) at the second test case, in spite of severe voltage dip fault and high wind penetration level, because of low fault duration (0.15 s).

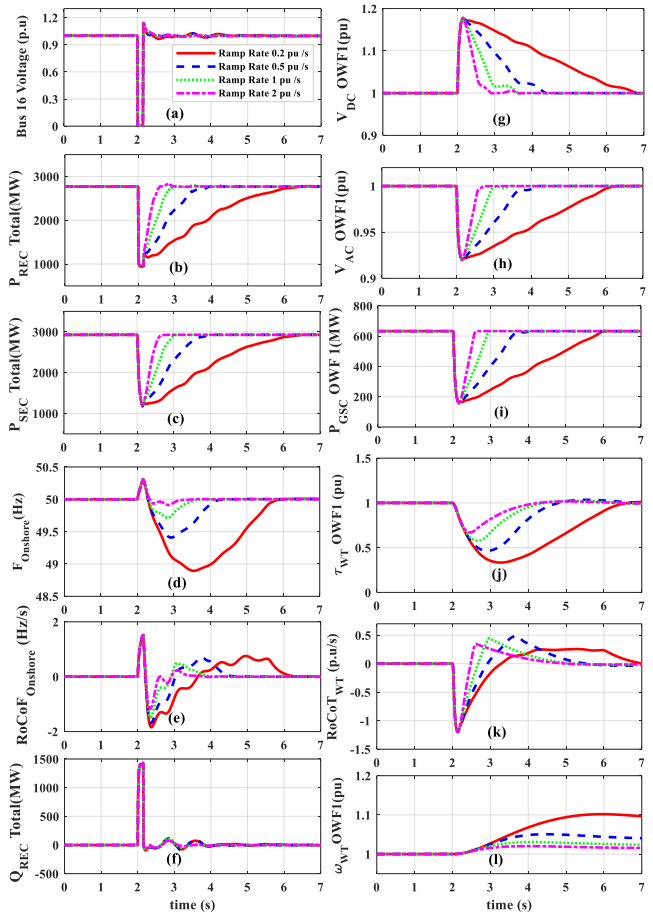

Fig .8 System performance under case study-II. (a) Bus 16 Voltage, (b) REC Active Power, (c) SEC Active Power, (d) Onshore frequency, (e) RoCoF of onshore frequency, (f) REC Reactive Power, (g) Offshore DC Voltage of OWF 1, (h) Offshore AC voltage of OWF 1, (i) WTG GSC Active Power (j) WTG Mechanical Torque, (k) RoCoT of WTG, (l) WTG rotational speed

VI. Conclusion

The APR ramp rate requirement imposed under GCRs is to decrease the mechanical stresses on the wind turbine mechanical parts and to avoid the impacts on grid stability due to rapid APR from OWFs after fault clearance. However, the results suggest that the VDIF is significantly improved specially at high APR ramp rates. Moreover, the wind generation penetration levels and grid fault severity may significantly impact frequency stability of onshore main grid. On the WTG side the APR ramp rate has a different effect, as with increasing the APR ramp rate the RoCoT is increased, however the WTG rotational speed decreased. On the other hand, as not expected the WTG mechanical stress decreased slightly at high ramp rate during low duration severe voltage dip faults and high wind penetration levels.

Acknowledgement

The work presented in this paper was supported by Industrial Research & Consultancy Centre, IIT Bombay through project no. 15IRCCSG033.

References

[1] European Environmental Agency, "Europe's onshore and offshore wind energy potential," Copenhagen, Denmark, 2009.

[2] GWEC, "Global Wind Energy Report: Annual Market Update 2017," *Https://Gwec.Net/Policy-Research/Reports/*, p. 72, 2018.

[3] Wind Europe, "Offshore Wind in Europe: Key Trends and Statistics 2018," 2018.

[4] A. Reidy and R. Watson, "Comparison of VSC based HVDC and HVAC Interconnections to a Large Offshore Wind Farm," *IEEE Power Eng. Soc. Gen. Meet.*, no. 1, pp. 71–78, 2005.

[5] ENTSO-E, "Network Code on High Voltage Direct Current Connections and DC- connected Power Park Modules," April, 2014.

[6] National Grid Electricity Transmission NGET, "The grid code," *Natl. Grid Electr. Transm.*, no. 5, 2017.

[7] TenneT TSO GmbH, "Requirements for Offshore Grid Connections in the Grid of TenneT TSO GmbH," 2012.

[8] Tennet TSO GmbH, "Grid Code - High and extra high voltage," November, 2015.

[9] J. B. Ekanayake, G. Ramtharan, N. Jenkins, F. M. Hughes, and A. Arulampalam, "Fault ride through of fully rated converter wind turbines with AC and DC transmission systems," *IET Renew. Power Gener.*, vol. 3, no. 4, p. 426, 2009.

[10] B. Silva, C. L. Moreira, H. Leite, and J. A. Pecas Lopes, "Control strategies for AC fault ride through in multiterminal HVDC grids," *IEEE Trans. Power Deliv.*, vol. 29, no. 1, pp. 395–405, 2014.

[11] A. Egea-alvarez, A. Junyent-ferre, and N. Jenkins, "Operation and control of VSC-HVDC multiterminal grids for offshore wind," *in Proc. 14th Eur. Conf. EPE*, Sep. 2011, pp. 1–9.

[12] M. Mohammadi, M. Avendano-Mora, M. Barnes, and J. Y. Chan, "A study on Fault Ride-Through of VSC-connected offshore wind farms," *2013 IEEE Power Energy Soc. Gen. Meet.*, pp. 1–5, 2013.

[13] A. A. Van Der Meer, M. Ndreko, S. Member, M. Gibescu, and M. A. M. M. Van Der Meijden, "The Effect of the Offshore VSC-HVDC-Connected Offshore Wind Power Plants on AC / DC System Dynamics," vol. 31, no. 2, pp. 878–887, 2016.

[14] S. I. Nanou, G. N. Patsakis, and S. A. Papathanassiou, "Assessment of communication-independent grid code compatibility solutions for VSC-HVDC connected offshore wind farms," *Electr. Power Syst. Res.*, vol. 121, pp. 38–51, 2015.

[15] K. Clark, N. W. Miller, and J. J. Sanchez-gasca, "Modeling of GE Wind Turbine-Generators for Grid Studies," *GE Energy*, no. 4.5, 2010.

[16] M. Pöller and S. Achilles, "Aggregated Wind Park Models for Analyzing Power System Dynamics," in *4th International Workshop on Large-scale Integration of Wind Power and Transmission Networks for Offshore Wind Farms*, 2003, pp. 1–10.

[17] S. Dennetière *et al.*, "The CIGRE B4 DC Grid Test System," *CIGRE Electra Mag.*, 2013.

[18] P. Demetriou, M. Asprou, J. Quiros-Tortos, and E. Kyriakides, "Dynamic IEEE Test Systems for Transient Analysis," *IEEE Syst. J.*, vol. 11, no. 4, pp. 1–10, 2015.